Contemporary Engineering Sciences, Vol. 12, 2019, no. 4, 229 - 240
HIKARI Ltd, www.m-hikari.com
https://doi.org/10.12988/ces.2019.9829

Computer-Assisted Diagnosis of Actinic Keratosis in Dermatoscopic Images

B. Luna-Benoso

Instituto Politécnico Nacional. Escuela Superior de Cómputo. Av. Juan de Dios Batíz, esq. Miguel Othón de Mendizábal, Mexico City 07738, Mexico

J. C. Martínez-Perales

Instituto Politécnico Nacional. Escuela Superior de Cómputo. Av. Juan de Dios Batíz, esq. Miguel Othón de Mendizábal, Mexico City 07738, Mexico

M.E. Cruz Meza

Instituto Politécnico Nacional. Escuela Superior de Cómputo. Av. Juan de Dios Batíz, esq. Miguel Othón de Mendizábal, Mexico City 07738, Mexico

Abstract

Actinic Keratosis is a skin lesion that presents as a coarse and scaly patch due to frequent exposure to ultraviolet radiation, its importance lies in the fact that the lesion can become squamous cell skin cancer, so it is very important its treatments in early stages. Computer-assign diagnostic (CAD) system leads to a pre-diagnosis of the lesion based on information regarding clinical criteria. In this work it is proposed develop a CAD system that allows the identification of Actinic Keratosis in lesions of the skin by dermatoscopy images analysis using spatial domain methods and pattern recognition.

1. Introduction

Actinic Keratosis (AK) are cutaneous neoplasms resulting from the abnormal proliferation of epidermal keratinocytes, which commonly appear in areas exposed to ultraviolet radiation such as the arms, hands, face and neck. If it is not treated in time, it can become squamous cell carcinoma, being the second most common skin neoplasm after basal cell carcinoma, and the leading cause of death of non-melanoma skin cancer [1], the risk of mutating to a cancerous neoplasm is 0.075% to 0.096% due to AK lesion per year, increasing the probability of risk for people suffering from multiple AK lesions [2]. AK Is expressed as macules or erythematous that are progressively coated with an adherent squama.

Several CAD systems have been developed that have helped in the timely detection of lesions in the skin, some only focus on the part of images segmentation, being the first module for the complete development of a CAD system, on the other hand, other CAD systems propose all methodology carried out that allows from the segmentation of the images until the classification of these, next we will mention some works. Spyridonos et al [3] developed a method based on color texture to automatically discriminate the presence of the Actinic Keratosis in clinical photographs. García-Arroyo et al [4] focus solely on the segmentation of skins lesions, this is done by thresholding histogram a diffuse pixel classifier applied to dermatoscopic images. Noroozi et al [5] propose a method to discriminate basal cell carcinoma tumors from squamous cell carcinoma tumors in hispatological images of the skin using Z-transform features. Celebi et al [6] propose an automated method that allows the detection of irregular and unstructured areas of confluent blue pigmentation whit a white film in form of superimposed frosted glass using contextual pixel classification using decision trees. Russell et al [7] worked with the analysis in dermatoscopic skin lesions of the detection of melanoma, they used Gaussian mixture models, Bayesian classifier and vector support machines. Al-masni et all [8] propose an automatic technique that allows to segment skin lesions in dermatoscopic images and apply it to recognize melanoma skin cancer, the proposed technique is performed via full resolution convolutional networks. Hames et al [9] propose an automatic methodology using color space transformations and morphologic characteristics for the detection of Actinic Keratosis in clinical photographs.

This paper presents the methodology for the detection of Actinic Keratosis in dermatoscopic images. The work is divided as follows: section 1 shows the introduction, section 2 shows the basic concepts necessary for the development of the methodology, section 3 show the proposed model, section 4 shows the experiments and results, and in section 5 the conclusions.

2. Basic Concepts

Digital Image

An image is a two-dimensional function *f(x,y)*, with *(x,y)* coordinates in the Cartesian plane. The amplitude of f of a pair of coordinates *(x,y)* is called image intensity of that point in space. An image is digital if both f and the value of the amplitude of the x and y coordinates are finite and discrete [10]. Since a digital image is a function *f(x,y)* discretized in both spatial coordinates and amplitude, it is often represented as a two-dimensional matrix $F_{ij} = (f_{ij})_{H \times W}$, where H and W represent the size of the image, (referring H and W to the height an width of the image respectively) with $f_{ij} = f(x_i, y_j)$ (Figure 1).

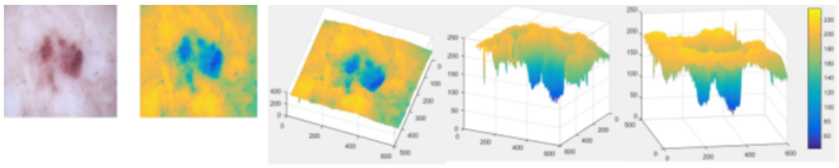

Fig 1: Digital image.

3. Proposed Model

The proposed model is divided into three modules: 1) segmentation of the lesion, 2) extraction of characteristics and 3) classification. Next, each of the modules that make up the methodology is presented.

3.1 Segmentation

This section presents the proposed methodology that allows the segmentation of lesions of dermatoscopic images applied to AK lesions. First, the RGB model of the decomposition of a digital image obtained from a digital dermatoscope is considered. An image must be composed of the superposition of its three RGB planes, that is, $I(x,y) = I_R(x,y) + I_G(x,y) + I_B(x,y)$. Four models were considered to obtain a grayscale image, first only the red plane was considered ($I_R(x,y) = R(x,y), I_G(x,y) = I_B(x,y) = 0$), secondly the green plane ($IG(x,y) = G(x,y), I_R(x,y) = I_B(x,y) = 0$), thirdly the blue plane ($I_B(x,y) = B(x,y), I_R(x,y) = I_G(x,y) = 0$), and fourthly the average of the three planes ($I_R(x,y) = R(x,y)/3, I_G = G(x,y)/3; I_B = B(x,y))/3$). The grayscale image that produced the best results is that of the blue plane, so all the proposed methodology was working on grayscale in the blue plane. Once

the grayscale was obtained, the optimal binarization threshold was calculated using the Otsu method. Figure 2 shows a grayscale color dermatoscopic image using its blue and binarized plane using the Otsu method.

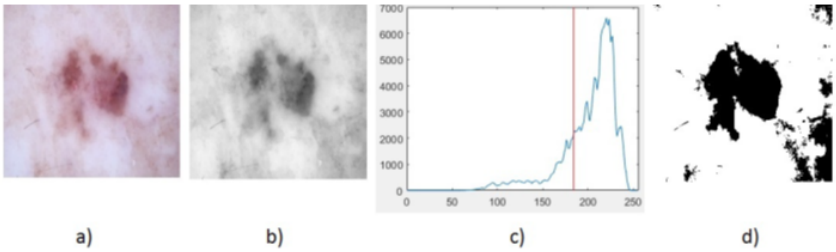

Fig 2: Digital image in a) color, b) grayscale, c) threshold by Otsu method and d) binarized image.

Once binarized image was obtained using the Otsu method, with the purpose of eliminating the noise, all those pairs of coordinates (x, y) such that $(C_x - x)^2 + (C_y - y)^2 \geq r^2$ were eliminated, where the point (C_x, C_y) is the center of the images and $r = min\{H/2, W/2\}$, this is:

$$f(x,y) = \begin{cases} 255 & \text{if} \quad (C_x - x)^2 + (C_y + y)^2 \geq r^2 \\ f(x,y) & \text{otherwise.} \end{cases} \tag{1}$$

Figure 3 shows in yellow the result of eliminating those points (x, y) that are outside the radius of the circumference.

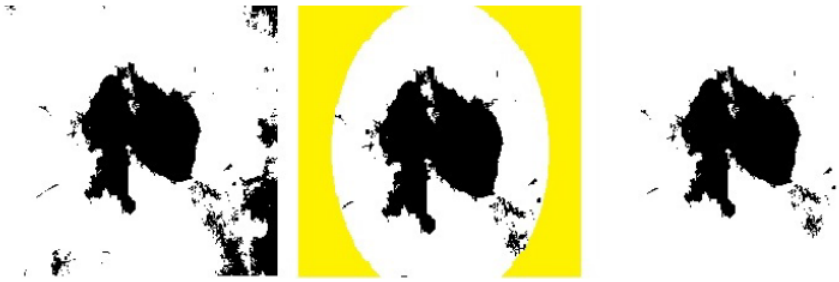

Fig 3: Elimination of points that are in the yellow zone.

Once those pixels that are outside the radius of the circle r have been eliminated, work is done on the segmented image obtained as in Figure 3 but in grayscale as shown in Figure 4: a) For each coordinate pair (i, j) of the image a mask of size L is taken, the function is considered: $g(i,j) = \sum_{(x,y)\in L_{(i,j)}} f(x,y)$,

where $L_{(i,j)}$ is the mask of size L transferred to the coordinate (i, j) and $f(i, j)$ the value of the grayscale image (Figure 4 b)). So that the resulting binary image is obtained as follows, for each coordinate pair (i, j), you have:

$$f(i,j) = \begin{cases} 255 & \text{if} \quad g(i,j) > 0.25L^2 \\ 0 & \text{otherwise.} \end{cases} \tag{2}$$

Figure 4 c) shows the result of applying the equation of the function (2) to the image of the Figure 4 a). Subsequently, a dilation was applied with a von Neumann neighborhood of size 9×9. Figure 4 d) shows the result of the dilation, Figure 4 e) shows the color segmented image, Figure 4 f) the contour of the segmented image and Figure 4 g) the contour of the segmented image on the color image.

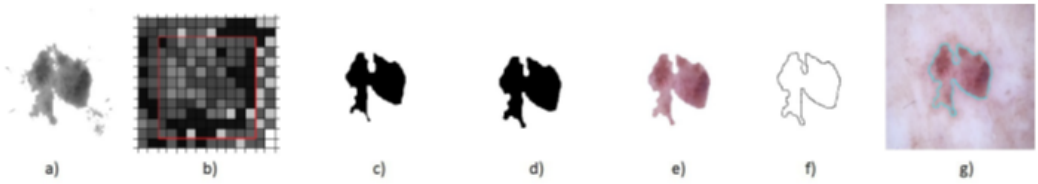

Fig 4: Obtaining the segmented image.

3.2 Feature Extraction

Once the image was segmented, a total of 11 statistical characteristics were extracted to form the patter that represents each image. Table 1 shows the statistical characteristics used, where N represents the total number of pixels, L is the total number of gray levels. $I(f_{ij})$ is the value of the gray level of the pixel (i, j) in the image $f(x, y)$, $P(j)$ is the probability that the value of the gray level j occurs in the image $f(x, y)$, $T(i)$ is the number of pixels with gray value i in the image $f(x, y)$, $P(I(f_{ij}))$ is the probability that the gray level $I(F_{ij})$ occurs in the image $f(x, y)$ and $P(f_{ij}) = T(I(f_{ij}))/N$.

3.2 Feature Extraction

For the classification, an associative model based on cellular automata (CA) was used. Associative models are mathematical models whose main objective is to recover complete patterns from input patterns. The operation of associative models is divider in two phases: learning phase, stage where associative model is generated; and recovery phase, stage in which associative model is operated [11, 12].

Characteristic	**Expression**
Mean	$\mu = \frac{\sum_{ij} f_{ij}}{N}$
Deviation Standard	$\sigma = \sqrt{\frac{\sum_{ij}(f_{ij}-\mu)^2}{N}}$
Smoothness	$R = 1 - \frac{1}{(1+\sigma^2)}$
Skewness	$\frac{\sum_{ij}(f_{ij}-\mu)^3}{N\sigma^3}$
Kurtosis	$\frac{\sum_{ij}(f_{ij}-\mu)^4}{(N-1)\sigma^4}$
Uniformity	$\sum_{i=0}^{L-1} P(i)^2$
Average Histogram	$AH_g = \frac{1}{L}\sum_{i=0}^{L-1} T(i)$
Modified Skew	$MSK = \frac{1}{\sigma^3}\sum_{ij}(f_{ij}-\mu)^3 P(f_{ij})$
Modified Standard Deviation	$\sigma_m = \sqrt{\sum_{ij}(f_{ij}-\mu)^2 P(f_{ij})}$
Entropy	$Etp = -\sum_{j=0}^{L-1} P(j) log_2[P(j)]$
Modified Entropy	$\sum_{ij} P(f_{ij}) log_2[P(I(f_{ij}))]$

Table 1: Statistical characteristics.

During the learning phase, associative model is constructed from a set of ordered pairs of previously known patterns, called the fundamental set. Each pattern that defines the fundamental set is called the fundamental pattern. The fundamental set is represented as follows [13]:

$$FS = (x^\mu, y^\mu)|\mu = 1, 2, \ldots, p \tag{3}$$

Where $(x^\mu, x^\mu) \in A^n x A^m$ for $\mu = 1, 2, \ldots p$, with $A = 0, 1$.

During the recovery phase, the associative model operates with a input pattern to obtain the corresponding output pattern.

In this work an associative model based on cellular automata presented by authors in [14] was used. Next, the learning and recovery phase of the proposed model is presented.

Consider the $CAQ = (L, S, N, f_Q)$ and $W = (L, S, N', f_W)$ with $N' = IJ$, and $f_Q : N \to S, f_W : N' \to S$ defined as follows:

$$f_Q(v^{(i,j)}) = \begin{cases} 1 & \text{if} \quad (i,j) \in L_{FS}; \\ 0 & \text{if} \quad (i,j) \notin L_{FS}; \end{cases}$$

$$f_W(v_{(i,j)}) = \begin{cases} 1 & \text{in position (i + 1,j)} \quad \text{if}(i, j-1) = 1; \\ 1 & \text{in position (i,j - 1)} \quad \text{if}(i+1, j) = 1; \end{cases}$$

We define the Associative $CA(ACA)$ in its learning phase as:

$W * Q = (L, S, N, f_A)$

Algorithm 1 ACA in recovery phase

Require: Fundamental set $FS = \{(x^\mu, y^\mu) \mid \mu = 1, 2, ..., p\}$; structuring element B; integer value ne (number of erosions); integer value nd (number of dilations); pattern recovery $\widetilde{x} \in A^n$
Ensure: Recovery pattern $\widetilde{y} \in A^m$

1. Building the Learning ACA for FS.

2. Applying ne times the cell erosion ε with the structuring element B to the initial configuration of learning ACA. This is, applied to the configuration of the $ACA, \varepsilon * \varepsilon * ... * \varepsilon, ne$ times.

3. Aplying nd times the cellular dilation with the structuring element D to configuration obtained in point 2. This is, applied to the configuration obtained in point $2, D * D * ... * D, nd$ times.

4. For the input pattern $\widetilde{x} \in An$ will get output pattern $\widetilde{y} \in A^m$ applying:

for $i = 1 \to m$ **do**
  $\widetilde{y} = 1$
  for $j = 1 \to n$ **do**
    if $\neg(\widetilde{x}_j = 0 \wedge (2j-1, 2i-2) = 1)$ **then**
      if$\neg(\widetilde{x}_J = 1 \wedge (2j-2, 2i-2) = 1 \vee (2j-1, 2i-2) = 1)$ **then**
        $\widetilde{y} = 0$
        $Break$
      end if
    end if
  end for
end for

The recovery phase for the ACA makes use of the composition of erosions and dilations CA. The algorithm which defines the phase of recovery is shown in algorithm 1.

4. Experiments and Results

The international Skin Imaging Collaboration (ISIC) is an academic project with the objective to develop tools for the analysis of images that allow the diagnosis of different types of skin lesions (nevus, basal cell carcinoma, dermatofibroma, melanoma and Actinic Keratosis among others) [15]. This work focused on lesions of Actinic Keratosis, in which a total of 206 dermatoscopic images were used, divided in 103 image that presented a lesion to be detected and 103 that presented some other type of lesion. Each of the dermatoscopic images used went through the segmentation process using the methodology

proposed in section 3.1. Subsequently, the statistical characteristics proposed in Table 1 were extracted. The associative model based on cellular automata presented in section 31 and in [14] was used. The proposed model was compared in K-NN classification algorithm, for this, their respective confusion matrices were first constructed. For K-NN, a value of k = 1, 3, 5 and 7 was used, and for the proposed model case a Moore neighborhood structuring element was used. Table 2 shows the confusion matrix for K-NN with different values of k and the associative algorithm AC, where $TP = TruePositive, FP = FalsePositive, TN = TrueNegativeandFN = FalseNegative.$

		True Condition Status	
		Positive	Negative
KNN (N=1)	Positive	TP=99	FP=20
	Negative	FN=4	TN=83
KNN (N=3)	Positive	TP=101	FP=1
	Negative	FN=2	TN=102
KNN (N=5)	Positive	TP=101	FP=7
	Negative	FN=2	TN=96
KNN (N=7)	Positive	TP=101	FP=9
	Negative	FN=2	TN=94
Proposed (AC)	Positive	TP=103	FP=3
	Negative	FN=0	TN=100

Table 2: Confusion matrix for KNN with different values of k and the proposed AC model.

Once the values in Table 2 were obtained, were calculated the metrics Sensitivity (SE), Specificity (SP) and Accuracy (ACC) metrics of nests were calculated as follows respectively:

$$SE = TP/(TP + FN) \tag{5}$$

$$SP = TN/(TN + FP) \tag{6}$$

$$ACC = (TN + TP)/(FN + FP + TN + TP) \tag{7}$$

From the values obtained in equations (5) and (6), the ROC curves that determine the accuracy of the model diagnosis are constructed. Figure 5 shows the result of the ROC curves for the K-NN algorithm, with k = 1,3,5 and 7, and for the proposed AC algorithm.

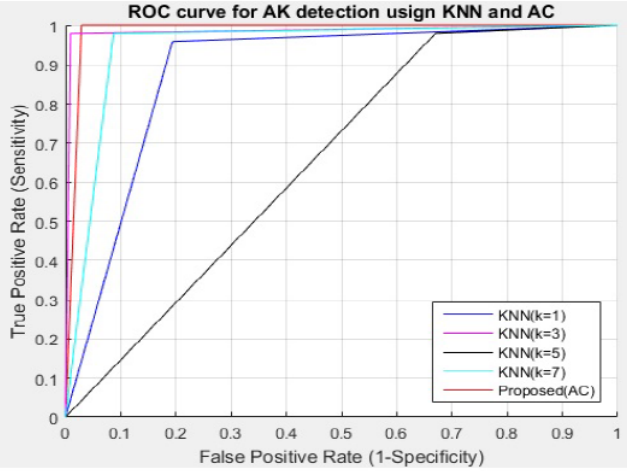

Fig 5: ROC curves for different KNN k values and the proposed AC algorithm.

Table 3 shows the comparison of the values obtained from ACC, SE and SP for the K-NN algorithm with different values of k, and the proposed AC algorithm.

Classifier	ACC	SE	SP
K-NN (k=1)	0.883	0.9611	0.8059
K-NN (k=3)	0.985	0.98	0.991
K-NN (k=5)	0.956	0.98	0.933
K-NN (k=7)	0.946	0.98	0.913
Proposed (AC)	**0.985**	**1**	**0.97**

Table 3: Comparison of AK diagnosis methods.

It is observed in Figure 5, that the ROC curve of the proposed AC model is above each of the ROC curves that the K-NN model throws for different values of k, the same happens with the sensitivity value shown in the Table 3. However, the value of the specificity is higher when using the K-NN model with $k = 3$, secondly is the AC model, however it is observed that the accuracy shown by the AC model is 0.985, the same that in the case $k = 3$ of the K-NN, both cases show the same accuracy and superior to other cases of the K-NN algorithm.

5. Conclusions

Currently, CAD systems have been developed in different areas of medicine with the aim of supporting pre-diagnosis in the medical area. This paper shows

the proposal of a CAD system that allows the detection of Actinic Keratosis in skin lesions of dermatoscopic images. The work was divided in three modules: 1) segmentation of the lesion, 2) extraction of characteristic and 3) classification. Methods in the spatial domain were used for the segmentation module, 11 statistical characteristics were sued for the feature extraction module, and a model base on cellular automata was used for the classification module and compared with the K-NN algorithm for different values of k, using the values produced by de confusion matrix, the ROC curves and the metrics of Sensibility (SE), Specificity (SP) and Accuracy (ACC). The AC model showed an accuracy of 0.985, just like the K-NN algorithm for $k = 3$, this value was higher than those shown for the other k-values of K-NN. It is also observed that the ROC curve for the AC model is above each of the ROC curves of the K-NN model from the 1 - SP value, since for previous values, the ROC curve for $k = 3$ is by above, this compensates for the fact that both algorithms showed an accuracy of 0.985. The exposition in this work shows that the AC algorithm yields acceptable results in comparison to the K-NN algorithm applied to the detection of skin lesions of the Actinic Keratosis.

Acknowledgements. The authors would like to thank the Instituto Politécnico Nacional (Secretaría Académica, COFAA, EDD, SIP and ESCOM) for their economical support to develop this work.

References

[1] Fernández-Figueras M.T., Carrato C., Senz X., Puig L., Musulen E., Ferndiz C., Ariza A., Actinic Keratosis with atypical basal cells (AK I) is the most common lesion associated with invasive squamous cell carcinoma of the skin, *J. Eur. Acad. Dermatol. Venereol.*, **29** (5) (2015), 991-997. https://doi.org/10.1111/jdv.12848

[2] Huerta-Brogeras M., Olmos O., Jess Borbujo et al., Validation of Dermoscopy as a Real-time Noninvasive Diagnostic Imaging Technique for Actinic Keratosis, *Arch. Dermatol.*, **148** (10) (2012), 1159-1164. https://doi.org/10.1001/archdermatol.2012.1060

[3] Spyridonos P., Gaitanis G., Likas A., Bassukas I. D., Automatic discrimination of actinic keratoses from clinical photographs, *Computers in Biology and Medicine*, **88** (2017), 50-59. https://doi.org/10.1016/j.compbiomed.2017.07.001

[4] Garcia-Arroyo J. L., Garcia-Zapirain B., Segmentation of skin lesions in dermoscopy images using fuzzy classification of pixels and histogram thresholding, *Computer Methods and Programs in Biomedicine*, **168** (2019), 11-19. https://doi.org/10.1016/j.cmpb.2018.11.001

[5] Noroozi N., Zakerolhosseini A., Computer assisted diagnosis of basal cell carcinoma using Ztransform features, *Journal of Visual Communication and Image Representation*, **40**, part A (2016), 128-148. https://doi.org/10.1016/j.jvcir.2016.06.014

[6] Celebi M. E., Iyatomi H., William V. Stoecker, Randy H. Moss, Soyer H. P., Automatic detection of blue-white veil and related structures in dermoscopy images, *Computerized Medical Imaging and Graphics*, **32**, issue 8 (2008), 670-677. https://doi.org/10.1016/j.compmedimag.2008.08.003

[7] Russell C. H, Redha A., Manawaduge S. Temesguen Messay Kebede, Skin Lesion Segmentation and Classification for ISIC 2018 Using Traditional Classifiers with Hand-Crafted Features, *Electrical Engineering and Systems Science*, ISIC 2018.

[8] Al-masni M. A, Al-antari M. A, Mun-Taek C., Seung-Moo H., Tae-Seong K., Skin lesion segmentation in dermoscopy images via deep full resolution convolutional networks, *Computer Methods and Programs in Biomedicine*, **162** (2018), 221-231. https://doi.org/10.1016/j.cmpb.2018.05.027

[9] Hames S. C., Sinnya S., Tan J. M, Morze C., Sahebian A., Soyer H. P., Prow T. W., Automated detection of actinic keratoses in clinical photographs, *PLoS One*, **10** (1) (2015), 112. https://doi.org/10.1371/journal.pone.0112447

[10] Gonzalez R, Woods J., Digital Image Processing, 3rd edn. Prentice Hall, New Jersey, 2008.

[11] Román-Godinez I., López-Yánez I., Yánez-Márquez C., Classifying Patterns in Bioinformatics Databases by Using Alpha-Beta Associative Memories, *Biomedical Data and Applications Studies in Computational Intelligence*, **224** (2009), 187-210. https://doi.org/10.1007/978-3-642-02193-0_8

[12] Vázquez R. A., Sossa H., Behavior of morphological associative memories with truecolor image patterns, *Neurocomputing*, **73** (13) (2009), 225-244. https://doi.org/10.1016/j.neucom.2009.09.004

[13] Aldape-Pérez M., Yáñez-Márquez C., Camacho-Nieto O., Arguelles-Cruz A.J., An associative memory approach to medical decision support systems, *Computer Methods and Programs in Biomedicine*, **106** (3) (2012), 287-307. https://doi.org/10.1016/j.cmpb.2011.05.002

[14] Luna-Benoso B., Flores-Carapia R., Yáñez Marquez C., Associative Memories Based on Cellular Automata: An Application to Pattern Recognition, *Applied Mathematical Sciences*, **7** (18) (2013), 857-866. https://doi.org/10.12988/ams.2013.13077

[15] International Skin Imaging Collaboration (ISIC), ISIC Archive, https://isic-archive.com

Received: September 11, 2019; Published: October 11, 2019